NASA Technical Memorandum 105435
ICOMP-92-03

ULTRA-SHARP Solution of the Smith-Hutton Problem

B.P. Leonard
Institute for Computational Mechanics in Propulsion
Lewis Research Center
Cleveland, Ohio

and

Simin Mokhtari
Department of Mechanical Engineering
The University of Akron
Akron, Ohio

February 1992

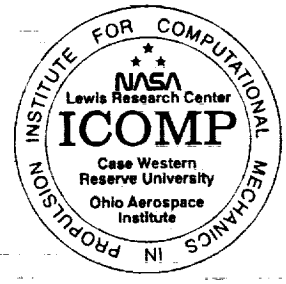

NASA

ULTRA-SHARP SOLUTION OF THE SMITH-HUTTON PROBLEM

B.P. Leonard*
Institute for Computational Mechanics in Propulsion
Lewis Research Center
Cleveland, Ohio 44135
and
Simin Mokhtari
Department of Mechanical Engineering, The University of Akron
Akron, Ohio

SUMMARY

Highly convective scalar transport involving near-discontinuities and strong streamline curvature was addressed in a paper by Smith and Hutton in 1982, comparing several different convection schemes applied to a specially devised test problem. First-order methods showed significant artificial diffusion, whereas higher-order methods gave less smearing but had a tendency to overshoot and oscillate. Perhaps because unphysical oscillations are more obvious than unphysical smearing, the intervening period has seen a rise in popularity of low-order artificially diffusive schemes, especially in the numerical heat-transfer industry. The present report describes an alternative strategy of using non-artificially diffusive higher-order methods, while maintaining strictly monotonic transitions through the use of simple flux-limiter constraints. Limited third-order upwinding is usually found to be the most cost-effective basic convection scheme. Tighter resolution of discontinuities can be obtained at little additional cost by using automatic adaptive stencil expansion to higher order in local regions, as needed.

1. INTRODUCTION

In a well-known paper published in 1982, Smith and Hutton presented results of several authors' attempts to numerically solve a specially devised test problem involving streamline curvature typical of recirculating flows and steep variations in the transported scalar[1]. Most schemes were able to handle the diffusion-dominated low-Peclet-number regime adequately; but in the important high-convection regime, Smith and Hutton concluded that convection modelling "remains the art of compromise between diffusive and oscillatory errors." In the intervening period, it seems that artifically diffusive low-order (blended first/second-order) convection schemes have become more popular than higher-order potentially oscillatory methods. Perhaps this is because the overshoot (or undershoot) problems associated with higher-order methods can lead to *obviously* unphysical results such as locally negative densities or absolute temperatures, for example. But the low-order methods' results are also usually highly unphysical — although perhaps not always obviously so.

Convection-diffusion schemes that revert to first-order upwinding for convection (while physical diffusion is ignored) under high-convection conditions achieve (plausible looking) nonoscillatory results by replacing the high-convection physical problem, with an artifically

*Work funded by Space Act Agreement C-99066-G.

diffusive (and anisotropic) *low*-convection numerical problem. Blended first/second-order schemes of this type, such as Spalding's "Hybrid" method[2] and Patankar's "Power-Law Difference Scheme" (PLDS)[3] seem to have gained in popularity in recent years, especially in the numerical convective heat-transfer industry[4]. This is puzzling, because there have been several studies showing the artificially diffusive nature of such schemes[5-10] over the past decade or more. Even more puzzling is the fact that many authors use Hybrid, PLDS or similar exponential-based schemes[11] in combination with sophisticated (and expensive) multiple-equation turbulence models — apparently not realizing that the turbulence model is being used throughout most of the flow-field merely as an expensive diagnostic to *switch-off* the physical (turbulent plus laminar) diffusion terms in the governing equations, replacing them with (anisotropic) artificial numerical diffusion. It is perhaps not surprising that the results of such computations are typically very insensitive to the turbulence model being used. Most puzzling of all is that some researchers continue to use first-order-based convection schemes to actually develop and "tune" new turbulence models.

The usual "justification" for this approach seems to be based on grid-refinement studies, i.e., the grid is refined to a point where the results do not seem to be changing very much. But, for first-order methods, the approach to true grid-independence is a notoriously slow process. One cannot claim reasonable accuracy (or proper use of the turbulence model) until the grid is refined to a point where the component grid Peclet (or Reynolds) numbers are everywhere $O(1)$ or less — in which case Hybrid and PLDS are operating as second-order central differencing. The massive grid refinement that this would call for under high-convection conditions is clearly impracticable.

There is a strong need for a conceptually simple (and computationally inexpensive) convection scheme giving highly accurate non-artificially diffusive and non-oscillatory results on practical grids under high-convection conditions; i.e., for grid Peclet (or Reynolds) numbers arbitrarily large. The same scheme should, of course, be able to handle the low-Peclet-number diffusion-dominated regime, as well. As will be shown in this report, these apparently conflicting requirements are not incompatible. Third-order upwinding is the lowest-order convection scheme for which the leading truncation error is dissipative (involving even-order spatial derivatives) but not "diffusive" (i.e., second-order derivatives) — by definition, leading truncation error in this case involves fourth-order spatial derivatives. As is well known, however, third-order upwinding in its basic form can give rise to unphysical overshoots or undershoots near regions involving rapid changes in the transported variable.

But it is a relatively simple matter to incorporate universal limiter constraints (applicable to any order of accuracy) giving tight monotonic resolution of near-discontinuities without corrupting the accuracy of the underlying scheme. This universal limiter for tight resolution and accuracy implemented *via* a simple high-accuracy resolution program constitutes the ULTRA-SHARP strategy for high-convection modelling. The recommended method uses limited third-order upwinding (ULTRA-QUICK) as the basic convection-diffusion scheme; then, in local regions requiring even higher-order resolution, the algorithm automatically branches to a limited higher-order scheme (ULTRA-5th or ULTRA-7th upwind, for example) using adaptive stencil expansion, locally, controlled by a simple non-smoothness monitor. In terms of achieving a desired accuracy (compared with a known

exact solution, for example), this strategy is optimal in terms of requiring the lowest computer cost as the grid is refined. In other words, although low-order methods are less expensive per grid point, they require an exorbitantly fine grid to achieve a prescribed accuracy; by contrast, the higher cost (per grid point) of very high-order methods used globally is not completely offset by the lower cost of a concomitantly coarser grid.

In the following sections the Smith-Hutton test problem is briefly described. Then, for reference, results are shown for a number of well-known convection-diffusion schemes; in particular: PLDS (representative of exponential-based schemes), second-order upwinding, and third-order upwinding (QUICK), using a conservative control-volume time-marching formulation. Fifth- and seventh-order upwinding are also briefly discussed; as is typical of unlimited higher-order schemes, tighter resolution in this case is offset by stronger oscillations. The concept of the universal limiter, based on normalized variables, is then briefly reviewed. Results are shown for limited third-order (ULTRA-QUICK) and an ULTRA-3rd/5th/7th-order scheme using local adaptive stencil expansion. Finally, a cost-effectiveness study shows the optimality of the third-order-based ULTRA-SHARP schemes.

2. TEST PROBLEM

The two-dimensional test problem devised by Smith and Hutton is concerned with steady-state convection and diffusion of a scalar field such as temperature, T, for example, in a prescribed velocity field, $\mathbf{v}(x, y)$, with a known constant diffusivity, D. The nondimensional governing equation is

$$\mathbf{v} \cdot \nabla T = \frac{1}{\mathrm{Pe}} \nabla^2 T \tag{1}$$

introducing the (macroscopic) Peclet number

$$\mathrm{Pe} = \frac{V_{\mathrm{ref}} L_{\mathrm{ref}}}{D} = \mathrm{const} \tag{2}$$

using appropriate reference velocity and length scales. The flow domain considered is a rectangle: $-1 \le x \le 1$, $0 \le y \le 1$. And the velocity field is given by

$$u = 2y (1 - x^2) \tag{3}$$

and

$$v = -2x (1 - y^2) \tag{4}$$

corresponding to a streamfunction

$$\psi = -(1 - x^2)(1 - y^2) \tag{5}$$

Figure 1 shows the streamline pattern for this flow-field.

The inlet temperature profile is specified as

$$T_{in}(x) = 1 + \tanh[\alpha(1 + 2x)] \tag{6}$$

for $y = 0$ and $-1 \leq x \leq 0$. This is also shown in Figure 1. For $x = -1$, the left-hand boundary condition becomes

$$T_b = T_{in}(-1) = 1 - \tanh \alpha \tag{7}$$

This is used as the boundary condition along the boundary streamline $\psi_b = 0$; i.e., at $x = \pm 1$ (for $0 \leq y \leq 1$) and at $y = 1$ (for $-1 \leq x \leq 1$). For α greater than about 3, this means that the boundary temperature is essentially zero, whereas the top of the inlet profile is very close to 2 as $x \to 0$. Smith and Hutton proposed $\alpha = 10$ as representative of a relatively sharp transition. In the present paper, two other values of α are used: $\alpha = 100$ (representative of a very sharp transition) and $\alpha = 5$ (representing a relatively smooth transition). Note that no physical boundary conditions are specified at the outlet boundary, $y = 0$ $(0 \leq x \leq 1)$. Numerical boundary conditions equivalent to

$$\left[\frac{\partial T}{\partial y}\right]_{y=0} = 0 \qquad \text{for} \quad 0 < x < 1 \tag{8}$$

are described below.

In the case of purely convective flow, $Pe \to \infty$, the exact solution is easily obtained, since $T = \text{const}$ along streamlines; i.e., $T = T(\psi)$. For example, at the inlet,

$$x = -\sqrt{1 + \psi}\,, \qquad -1 \leq x \leq 0 \tag{9}$$

so, throughout the flow domain when there is no diffusion,

$$T(\psi) = 1 + \tanh[\alpha(1 - 2\sqrt{1 + \psi})] = T(x, y) \tag{10}$$

using Equation (5). In particular, this gives an outlet profile as the mirror-image of the inlet profile

$$T_{out}(x) = 1 + \tanh[\alpha(1 - 2x)] \tag{11}$$

for $y = 0$ and $0 < x \leq 1$. Figure 2 shows a three-dimensional portrayal of Equation (10) on a 40×20 uniform mesh (41×21 grid-points, with $\Delta x = \Delta y$). In Figure 2(a), $\alpha = 100$; whereas in 2(b), $\alpha = 5$.

Figure 3 shows portions of a typical staggered mesh used in the present analysis. Note that T-nodes are placed at boundaries. Boundary nodes shown as dots within squares correspond to specified boundary conditions; solid dots represent interior computed T-nodes; exterior pseudo-T-nodes (triangles) are also shown for use with higher order methods. Hollow circles represent ψ-nodes; these occur at the corners of temperature control-volume cells. This is shown in more detail in Figure 4. This is a convenient arrangement, since *average* cell-face convecting velocities are then available by simple subtraction of stream-function values; e.g., referring to Figure 4,

$$u_l = \frac{\psi_{TL} - \psi_{BL}}{\Delta y} \tag{12}$$

so that the average left-face Courant number is

$$\mathrm{CXL}(i, j) = \frac{(\psi_{TL} - \psi_{BL})\ \Delta t}{\Delta x\ \Delta y} \tag{13}$$

Computation of interior node values of T follows a simple time-marching procedure. One first computes the left and bottom face fluxes

$$\mathrm{FLUXL}(i, j) = \mathrm{CXL} \cdot T_l - \frac{|\mathrm{CXL}|\ \Delta x}{\mathrm{PXL}} \left[\frac{\partial T}{\partial x}\right]_l \tag{14}$$

and

$$\mathrm{FLUXB}(i, j) = \mathrm{CYB} \cdot T_b - \frac{|\mathrm{CYB}|\ \Delta y}{\mathrm{PYB}} \left[\frac{\partial T}{\partial y}\right]_b \tag{15}$$

introducing local component cell face Peclet numbers

$$\text{PXL} = |u_t| \text{ Pe } \Delta x \tag{16}$$

and

$$\text{PYB} = |v_b| \text{ Pe } \Delta y \tag{17}$$

The new values of T are then updated by a simple assignment statement,

$$\begin{aligned} \text{Set: } T(i, j) = T(i, j) &+ \text{FLUXL}(i, j) - \text{FLUXL}(i+1, j) \\ &+ \text{FLUXB}(i, j) - \text{FLUXB}(i, j+1) \end{aligned} \tag{18}$$

where flux conservation has been observed at each face. This is repeated until a converged steady state has been achieved.

The treatment of the outflow numerical boundary condition is shown in Figure 5. Assume that $T(y)$ follows a parabola near the outlet for $y \geq 0$, with three conditions

$$T(2\Delta y) = T_2 \tag{19}$$

$$T(\Delta y) = T_1 \tag{20}$$

and

$$\left[\frac{\partial T}{\partial y}\right]_0 = 0 \tag{21}$$

Then, it is not hard to show that the corresponding value of T at the boundary is

$$T_0 = \frac{4}{3} T_1 - \frac{1}{3} T_2 \tag{22}$$

The corresponding pseudonode values of T_{-1} and T_{-2} (used for fifth- and seventh-order upwinding) are taken to be simply

$$T_{-1} = T_{-2} = T_0 \tag{23}$$

as shown in the figure. Pseudonode values along the other boundaries are set equal to their adjacent boundary values in a normal direction.

3. EXPONENTIAL-BASED SCHEMES

Exponential-based convection-diffusion schemes were first introduced into computational fluid dynamics by Allen and Southwell[12], and have been "rediscovered" in various equivalent or approximate formulations by several people in the past thirty-five years. Spalding's Hybrid scheme[2], Patankar's PLDS[3], and the algebraic approximation of Raithby and Schneider[11] can be interpreted as various levels of approximation to the exponential differencing scheme (EDS). It is fairly easy to show[13] that EDS is equivalent to using second-order central differencing for both convective and diffusive fluxes while replacing the actual grid Peclet (or Reynolds) number, P_Δ, with an effective value, P_Δ^*, that is itself a function of the physical P_Δ. The functional relationship is[13]

$$P_\Delta^* = 2 \tanh(P_\Delta/2) \tag{24}$$

Spalding's Hybrid scheme can be interpreted as a very rough approximation to this, given by

$$\left.\begin{aligned} P_\Delta^* &= P_\Delta \qquad \text{for} \quad 0 \le P_\Delta \le 2 \\ P_\Delta^* &\equiv 2 \qquad \text{for} \quad P_\Delta > 2 \end{aligned}\right\} \tag{25}$$

Patankar's power-law difference scheme represents a much more accurate approximation of the hyperbolic-tangent function

$$\left.\begin{aligned} P_\Delta^* &= \frac{2P_\Delta}{P_\Delta + 2(1 - 0.1\,P_\Delta)^5} \qquad \text{for} \quad 0 \le P_\Delta \le 10 \\ P_\Delta^* &\equiv 2 \qquad \text{for} \quad P_\Delta > 10 \end{aligned}\right\} \tag{26}$$

The algebraic formulation of Raithby and Schneider can be interpreted as

$$P_\Delta^* = \left[\frac{P_\Delta^2}{2(5 + P_\Delta^2)} + \frac{(1 + 0.005\,P_\Delta^2)}{P_\Delta(1 + 0.05\,P_\Delta^2)}\right]^{-1} \tag{27}$$

Note that here, too, $P_\Delta^* \to 2$ for large values of P_Δ. In fact, for EDS itself, Equation (24), $P_\Delta^* \approx 2$ for $P_\Delta > 6$ (since $\tanh 3 = 0.995\ldots$). All three approximations are shown in relation to the hyperbolic-tangent curve in Figure 6.

For exponential-based schemes, the left-face flux, for example, is given by

$$\text{FLUXL}(i, j) = \frac{\text{CXL}}{2} (T_{i,j} + T_{i-1,j}) - \frac{|\text{CXL}|}{\text{PXL}^*} (T_{i,j} - T_{i-1,j}) \tag{28}$$

where PXL^* is the effective local x-component grid Peclet number at the left face. Note that for $\text{PXL}^* = 2$, the flux becomes

$$\text{FLUXL}(i, j) = \text{CXL} \cdot T_{i-1,j} \qquad \text{for} \quad \text{CXL} > 0 \tag{29}$$

or

$$\text{FLUXL}(i, j) = \text{CXL} \cdot T_{i,j} \qquad \text{for} \quad \text{CXL} < 0 \tag{30}$$

This, of course, corresponds to first-order upwinding for convection, with physical diffusion (computed but) ignored. This is what occurs in the Hybrid scheme for $P_\Delta > 2$, and in the other schemes (including EDS) for P_Δ greater than about 6.

Figure 7 shows 40×20 results for $\text{Pe} = \infty$; in this case the scheme is operating everywhere as first-order upwinding. By comparison with Figure 2, these are seen to be very artificially diffusive results. This is typical of exponential-based schemes. Figure 8 gives inlet and outlet profiles using $\alpha = 100$ for $\text{Pe} = \infty$, 500, and 10, showing computed solutions on 20×10, 40×20, and 80×40 grids in each case, using PLDS. The reference finite-Peclet-number results have been obtained using the ULTRA-3/5/7 upwind scheme (described later) on a very fine (160×80) grid. For the larger-Pe cases, the gross artificial diffusion of the exponential-based scheme is clear. In the case of $\text{Pe} = 10$, local *grid* Peclet numbers are small and the scheme is equivalent to second-order central differencing. The error reported in the figure captions is computed using

$$\mathscr{E} = \frac{1}{N} \sum |T_{\text{comp}} - T_{\text{ref}}| \tag{31}$$

where the summation is over all interior grid-points plus the outlet boundary, and N is the total number of grid-points involved, excluding pseudonodes (i.e., $N = 21 \times 11$, 41×21, or 81×41).

4. SECOND-ORDER UPWINDING

When second-order upwinding is used for convection, it is conventional to use second-order central differencing for diffusion. In this case, the left-face flux, for example, is given by

$$\text{FLUXL}(i, j) = \text{CXL} \cdot T_\ell - \frac{|\text{CXL}|}{\text{PXL}} (T_{i,j} - T_{i-1,j}) \tag{32}$$

where the left-face convected value is

$$T_\ell = \frac{3}{2} T_{i-1,j} - \frac{1}{2} T_{i-2,j} \qquad \text{for} \quad \text{CXL} > 0 \tag{33}$$

or

$$T_\ell = \frac{3}{2} T_{i,j} - \frac{1}{2} T_{i+1,j} \qquad \text{for} \quad \text{CXL} < 0 \tag{34}$$

Similar formulas are easily obtained for the bottom-face flux. Equations (33) and (34) can be combined into a single form valid for positive and negative convecting velocities by writing

$$T_\ell = \frac{1}{2} (T_{i,j} + T_{i-1,j}) - \frac{1}{2} \text{CURVNL} \tag{35}$$

defining the "normal curvature" at the left face as

$$\text{CURVNL} = \text{CRVAVL} - \frac{\text{SGN(CXL)}}{2} \text{THIRDL} \tag{36}$$

where (suppressing the j-index, for convenience) the average (symmetric) second-difference across the left face is

$$\text{CRVAVL} = \frac{1}{2} (T_{i+1} - T_i - T_{i-1} + T_{i-2}) \tag{37}$$

and the third-difference across the face is

$$\text{THIRDL} = T_{i+1} - 3T_i + 3T_{i-1} - T_{i-2} \tag{38}$$

The infinite-Pe results for second-order upwinding are shown in Figure 9 — as usual, for $\alpha = 100$ and 5. In this case, the smooth-inlet-transition results are quite good, with only a little numerical spreading and a very slight overshoot near the outlet; but note the significant overshoots and undershoots in the sharp-transition case. Figure 10 shows grid-dependence results for $\text{Pe} = \infty$, 500, and 10, for $\alpha = 100$.

5. THIRD-ORDER UPWINDING (QUICK)

The QUICK scheme (quadratic upstream interpolation for convective kinematics) is the canonical third-order-upwind scheme for steady-state flow[14]. In this case, the left-face flux, for example, has the same form as Equation (32); however, for consistency, the convected face value includes both normal and *transverse* curvature effects[14] and the normal-curvature coefficient is much smaller

$$T_f = \frac{1}{2}(T_{i,j} + T_{i-1,j}) - \frac{1}{8}\,\text{CURVNL} + \frac{1}{24}\,\text{CURVTL} \tag{39}$$

where CURVNL is given by Equation (36) and the upwind-weighted transverse-curvature term is

$$\text{CURVTL} = T_{i-1,j+1} - 2T_{i-1,j} + T_{i-1,j-1} \qquad \text{for} \quad \text{CXL} > 0 \tag{40}$$

or

$$\text{CURVTL} = T_{i,j+1} - 2T_{i,j} + T_{i,j-1} \qquad \text{for} \quad \text{CXL} < 0 \tag{41}$$

Note that, consistent with bi-quadratic interpolation in the vicinity of the left face, the diffusive flux is identical to that obtained by central-differencing[14].

The QUICK results for $\text{Pe} = \infty$ are shown in Figure 11. The smooth-transition case is very well modelled; but, as with second-order upwinding, overshoots and undershoots occur in the sharp-transition simulation, although the computed transition itself is noticeably sharper in this case. Grid-dependence results are seen in Figure 12.

6. FIFTH- AND SEVENTH-ORDER UPWINDING

The fifth-order upwind algorithm used in this paper again takes the form of Equation (32), but in this case

$$T_t = \frac{1}{2}(T_{i,j} + T_{i-1,j}) - \frac{1}{6}\,\mathrm{CRVAVL} + \frac{3}{128}\,\mathrm{FORTHL} + \frac{1}{24}\,\mathrm{CURVTL} \qquad (42)$$

where (again suppressing j's for convenience) the upwind-weighted fourth difference is

$$\mathrm{FORTHL} = T_{i+1} - 4T_i + 6T_{i-1} - 4T_{i-2} + T_{i-3} \qquad \text{for} \quad \mathrm{CXL} > 0 \qquad (43)$$

or

$$\mathrm{FORTHL} = T_{i+2} - 4T_{i+1} + 6T_i - 4T_{i-1} + T_{i-2} \qquad \text{for} \quad \mathrm{CXL} < 0 \qquad (44)$$

Three points should be mentioned:

(i) Higher-order terms are not used in the diffusive flux. This is appropriate because, when diffusion is large (small Pe), modelled profiles are smooth and the second-order form is entirely adequate; whereas, under high-convection conditions, the form of the small diffusion terms is not very important.

(ii) Higher-order transverse terms are not used in the convective flux. Although the third-order transverse curvature term is significant, numerical experimentation has shown that higher-order transverse terms have an almost negligible effect on results; but inclusion would add significantly to the cost of the calculation.

(iii) The coefficient of the normal-curvature term (1/6, rather than the theoretical value of 1/8) has been found to give slightly more accurate results in cases of scalar convection and diffusion, where exact solutions are available[13]. This was not found to be the case with third-order upwinding — where 1/8 seems to be optimal in all cases tested.

Figure 13 gives the fifth-order results for $\mathrm{Pe} = \infty$. As perhaps expected, the large-α transition is sharper (than third-order) but generates significantly more overshoots, undershoots, and secondary ripples. The smooth transition is graphically indistinguishable from the exact result. Grid-dependence studies are again predictable and need not be shown here. Higher (for example, seventh) order upwinding merely accentuates the trends seen with fifth-order.

The seventh-order formula used in this study takes the form

$$T_f = \frac{1}{2}(T_{i,j} + T_{i-1,j}) - \frac{1}{6}\,\mathrm{CRVAVL} + \frac{3}{128}\,\mathrm{FTHAVL} - \frac{1}{100}\,\mathrm{SIXTHL} + \frac{1}{24}\,\mathrm{CURVTL} \tag{45}$$

where (suppressing j's, as usual) the average (symmetric) fourth-difference across the left-face is

$$\mathrm{FTHAVL} = \frac{1}{2}(T_{i+2} - 3T_{i+1} + 2T_i + 2T_{i-1} - 3T_{i-2} + T_{i-3}) \tag{46}$$

and SIXTHL is the upwind-weighted sixth-difference

$$\mathrm{SIXTHL} = T_{i+2} - 6T_{i+1} + 15T_i - 20T_{i-1} + 15T_{i-2} - 6T_{i-3} + T_{i-4} \tag{47}$$

for CXL > 0; all indexes in SIXTHL are increased by 1 for CXL < 0.

7. UNIVERSAL LIMITER

The universal limiter is most easily described in terms of normalized variables. Let T_f represent the value of the convected scalar at any control-volume face; call the adjacent downstream node value T_D, the adjacent upstream node value T_C, and the next upstream node value (in a direction normal to the face) T_U. Figure 14 sketches the definition of these terms; as seen, node C lies between nodes U and D. Note, however, that the nodes involved are dependent on the sign of the normal convecting velocity component, u_n, at the CV face. Now define, anywhere in the vicinity of the face, a normalized variable

$$\tilde{T}(x, y) = \frac{T(x, y) - T_U}{T_D - T_U} \tag{48}$$

In particular,

$$\tilde{T}_f = \frac{T_f - T_U}{T_D - T_U} \tag{49}$$

and

$$\tilde{T}_C = \frac{T_C - T_U}{T_D - T_U} \tag{50}$$

Note also that $\tilde{T}_U = 0$, whereas $\tilde{T}_D = 1$.

The universal limiter can be portrayed in the $(\tilde{T}_C, \tilde{T}_f)$ plane[13]. Figure 15 shows the constraint boundaries. Note that first-order upwinding $(\tilde{T}_f = \tilde{T}_C)$ marginally satisfies the limiter constraints. Use of the universal limiter proceeds as follows:

(i) First compute some (in general, high-order) estimate for the face value, T_f, and find the corresponding normalized values of $\tilde{T}_f$ and $\tilde{T}_C$.

(ii) If the point $(\tilde{T}_C, \tilde{T}_f)$ satisfies the limiter constraints, proceed to step (iii); if not, reset $\tilde{T}_f$ to the nearest limiter-constraint at the same $\tilde{T}_C$ value.

(iii) Reconstruct the unnormalized face value

$$T_f = \tilde{T}_f (T_D - T_U) + T_U \tag{51}$$

(iv) Use this value in combination with second-order diffusion in computing the total flux at the CV face; as, for example, in Equation (32) for the left face.

ULTRA-QUICK Results

When the universal limiter (for tight resolution and accuracy) is applied to the QUICK scheme (giving ULTRA-QUICK), overshoots and undershoots are automatically suppressed without additional smearing of the transition region. This is seen in Figures 16 and 17 — which should be compared with Figures 11 and 12, and with Figure 2. Note the clean monotonic transition in the high-Pe large-α cases, as compared with the unlimited scheme. Smooth-region behaviour remains very good, reflecting the uniformly third-order accuracy of the basic algorithm.

Artificial Compression

Figure 18 portrays a second-order convection scheme in the normalized-variable diagram, conforming to universal limiter constraints. The unconstrained portion of the scheme (DCB) consists of second-order central-differencing (DC) for $\tilde{T}_C \leq 0.5$

$$\tilde{T}_f = \frac{1}{2} (1 + \tilde{T}_C) \tag{52}$$

and second-order upwinding (CB) for $\tilde{T}_C \geq 0.5$.

$$\tilde{T}_f = \frac{3}{2} \tilde{T}_C \tag{53}$$

The upper constraint boundary (BA) can be interpreted as first-order *down*winding

$$\tilde{T}_f = 1 \tag{54}$$

This convection scheme has a tendency to introduce *negative* artificial diffusion into portions of simulated profiles. This can (artificially) enhance resolution of near-discontinuities — a phenomenon sometimes known as ''artificial compression.'' The scheme was originally introduced by Roe[15] and named ''Ultra-B''; it is related to Roe's better-known ''Super-B'' scheme, which is also artificially compressive. In terms of simulating near-discontinuities, Ultra-B is indeed quite impressive for a second-order scheme. This is clearly seen in Figure 19(a) for the infinite-Pe sharp-transition case ($\alpha = 100$) ; but note the distortion of the initially smooth profile ($\alpha = 5$) in Figure 19(b). As the profile is convected downstream, it becomes more and more step-like. This is due to the negative artificial diffusion inherent in artificially compressive schemes. Similar artificial steepening effects occur with the finite-Pe simulations, as well. This is a serious draw-back of artificial-compression methods. The phenomenon can be avoided by using higher-order ULTRA-SHARP techniques, as described in the next section.

8. ADAPTIVE STENCIL EXPANSION

Higher-order monotonic resolution of very sharp transitions could be obtained by using ULTRA-5th or ULTRA-7th globally. But in most of the flow domain, such high accuracy (and concomitant cost) is not called for. It is of interest, from a cost-effectiveness viewpoint to construct an algorithm that would use ULTRA-QUICK in ''smooth'' regions and automatically branch to a higher-order scheme *locally*, as needed. The need for the higher-order calculation — and correspondingly expanded stencil — can be determined by monitoring some suitable ''non-smoothness'' parameter. One such quantity that comes to mind immediately is the local first-difference (proportional to the gradient) across a given CV face. For the left face, this would be

$$\text{GRADL} = T_{i,j} - T_{i-1,j} \tag{55}$$

One also needs to detect local *changes* in gradient; the symmetrically placed average second-difference, defined in Equation (37) for the left face, is suitable for this.

In smooth regions, both GRADL and CRVAVL will lie below certain pre-assigned thresholds; in this case, the basic ULTRA-QUICK algorithm is used — this will take care

of the bulk of the flow domain since sharp transitions occur in narrow isolated regions, by definition. If CRVAVL exceeds the first threshold, THC1 (= 0.1 in the present study), the algorithm branches to ULTRA-5th *locally*; if it also exceeds THC2 (= 0.7), it branches further to ULTRA-7th. If GRADL exceeds THG (= 0.35), ULTRA-7th is used immediately. Clearly, other threshold strategies could be used; the procedure adopted here has evolved through computational experimentation over several test problems. It should be noted that the threshold constants are dimensional; i.e., a change in scale, for example, would require a corresponding change in threshold values. This problem can be avoided by rescaling the threshold constants with respect to an anticipated maximum absolute value of the convected variable occurring within the flow-field of interest (in the Smith-Hutton problem $|T|_{max} = 2$).

Figures 20 and 21 show results for the ULTRA-3rd/5th/7th scheme described above. Clearly, these are highly accurate results, even on the coarsest grid. As seen in the next section, the cost is only slightly more than the basic ULTRA-QUICK scheme — but the *cost-effectiveness* (computational efficiency) is greatly enhanced.

9. OPTIMAL COST-EFFECTIVENESS

When dealing with higher-order convection schemes, one obvious question that comes to mind is: is it better (in terms of total cost) to use a low-order scheme on a very fine grid or a higher-order scheme on a coarser grid? Low-order schemes are relatively inexpensive per grid-point, but (as seen in the cases shown in this paper) require extremely fine grids for reasonable accuracy. On the other hand the added expense (again, per grid-point) of very-high-order schemes may not be totally offset by a concomitant coarsening of the grid. To be more precise, assume that a desired level of accuracy has been preassigned for a problem that has a known exact solution — such as the infinite-Pe Smith-Hutton problem. Take any given convection scheme and solve on successively finer and finer grids until the desired level of accuracy has been achieved; simultaneously keep note of the CPU time (representing cost) at successive grid refinements. Repeat this process with other convection schemes. In this way, the cost for a prescribed global accuracy can be assigned to each scheme. Alternatively, one could specify an available computational budget and compute the corresponding accuracy of each scheme as the grid is refined.

Figure 22 gives the relevant information for the infinite-Pe Smith-Hutton problem with $\alpha = 100$. In part (a) of the figure, the error, given by Equation (31), is plotted *versus* N, on a log-log scale, for first-order upwinding, ULTRA-second-order upwinding (equivalent to the Chakravarthy-Osher scheme described by Sweby[16]), ULTRA-QUICK, ULTRA-5th, and ULTRA-7th upwind schemes, together with the ULTRA-3rd/5th/7th upwind scheme. Desired accuracy is shown by a dashed line; for each scheme, the corresponding grid refinement can be found by interpolation. This is cross-plotted onto part (b) of the figure which gives CPU-time as a function of N for each scheme. Part (c) of the figure shows the error incurred by each method corresponding to a prescribed CPU-time in part (b). Alternatively, part (d) of the figure gives the CPU-time for each method corresponding to the prescribed error in part (a).

From these results, one sees immediately that first-order upwinding is extremely inefficient. Among the global higher-order methods, either ULTRA-QUICK or ULTRA-5th is seen to be optimal; the 7th-order scheme is significantly less efficient. The most cost-effective strategy of all, though, is to use adaptive stencil expansion over the base third-order scheme. This is because the wider-stencil (more expensive) higher-order computation is automatically used very sparingly — only where needed: in isolated narrow regions involving a relatively few number of grid points. For flows involving only relatively smooth profiles (such as the $\alpha = 5$ infinite-Pe case), ULTRA-QUICK is again found to be optimal; in this case, the higher-order wider stencil is not called for.

10. CONCLUSION

The Smith-Hutton problem is an excellent test of a numerical convection-diffusion scheme, especially in the high-convection regime. Strong streamline curvature and rapid local variation of the convected variable represent serious challenges to any numerical scheme. The availability of exact analytical solutions in the infinite-Pe case is very useful for a comparative error analysis. By choosing small values of α, the test-problem can be used for simulating smooth-function behaviour, as well. The present formulation of the problem uses a staggered grid, interleaving streamfunction and scalar nodes. Particular attention is paid to the outflow boundary condition, assuring $(\partial T/\partial y)_0 = 0$, consistent with local parabolic behaviour. The solution algorithm is based on explicit time-marching until a steady state is reached, although ADI tridiagonal solution of the steady equations can also be used[13].

Exponential-based schemes such as Spalding's Hybrid[2], Patankar's PLDS[3], or the algebraic approximation of Raithby and Schneider[11], all revert to first-order upwinding for convection with modelled physical diffusion (computed but) ignored or suppressed wherever the local component grid Peclet number exceeds 2 (Hybrid) or about 6 (for the other schemes, including EDS itself). For most flows of practical interest, the grid Peclet number is likely to be far greater than 2 or 6 throughout most of the flow-field; under these conditions, exponential-based schemes are functioning as first-order upwinding almost everywhere. The inherent artificial diffusion of such schemes is clearly evident, especially in the large-Pe cases. Slow grid-refinement convergence is also observed; this raises serious questions regarding grid-refinement claims made in support of exponential-based schemes. Such methods should be viewed as of historical interest only — and *should not be used* for serious practical applications.

Second-, third-, and higher-order upwind methods share a number of similar properties: as the order is increased, transition resolution becomes sharper, but overshoots and undershoots become more pronounced, with secondary ripples forming in the case of very-high-order schemes. Smooth function and low-Pe performance was seen to be generally very good, with error decreasing with order. The two-dimensional third-order (QUICK) scheme introduces transverse-curvature terms into the convective fluxes. Other calculations have shown that omission of these terms can incur significant error unless the grid is extremely fine. As used in this study, higher-order schemes retain the third-order transverse curvature terms but omit higher-order transverse and other cross-difference terms; these are costly,

algorithmically complex, and seem to have very little effect on the solution. It was also found unnecessary to extend diffusion modelling beyond second order.

The main draw-back of higher-order schemes is the generation of spurious unphysical overshoots and undershoots each side of sharp transition regions. This appears to be the main reason for a lack of interest in such methods as compared with essentially first-order schemes that produce monotonic, albeit extremely artificially diffusive, results. But it is a relatively straight-forward task to incorporate monotonizing flux-limiters into higher-order schemes, using the concept of a universal limiter, as described in § 7. In terms of locally normalized variables, the universal limiter diagram is a simple triangular region with linear extensions on each side. When applied to higher-order convective fluxes, the universal limiter produces strictly monotonic results without introducing artificial diffusion and concomitant numerical spreading of (what should be sharp) transition regions. The tightness of the transition resolution increases as the order of the underlying scheme is increased. Using a higher-order ULTRA scheme was seen to be a better strategy than relying on artificial compression. The negative artificial diffusion inherent in second-order artificial-compression methods such as Ultra-B is responsible for extremely tight resolution of near-discontinuities; however, as was seen, it tends to distort smooth profiles into a series of ramps and plateaus. In a recent paper, Tzanos[17] has also solved the Smith-Hutton problem using a third-order convection scheme with a simple limiting strategy essentially equivalent to ULTRA-QUICK (but without transverse curvature terms). Tzanos' paper also gives formulas for a variable (adaptive) grid. The results (for $\alpha = 10$ and $Pe = 1000$ or 10) are very similar to ULTRA-QUICK results for the same parameter values (slight differences are due to transverse-curvature terms and different treatment of numerical boundary conditions).

Among higher-order ULTRA schemes used globally, ULTRA-QUICK and ULTRA-5th were seen to be the best schemes in terms of cost-effectiveness: either lowest cost for a prescribed accuracy or lowest error for a prescribed cost, as the grid is refined. Adaptive stencil expansion — using ULTRA-QUICK as the base scheme and automatically expanding the computational stencil to a higher-order ULTRA scheme locally (as needed) — was seen to be an extremely cost-effective technique, giving between fifth- and seventh-order accuracy for little more cost than that of the underlying third-order scheme. Optimal setting of the non-smoothness monitor thresholds requires some experimentation for each new problem; but it appears likely that a more general strategy will evolve as experience is gained with this new technique.

The ULTRA-SHARP strategy is ideally suited to steady-state Navier-Stokes calculations, as well[18]. If a turbulence model is used, the physics of the model is faithfully represented. Very narrow shear-layers can be accurately simulated without fear of artificial smearing or oscillation. It is a straight-forward exercise to extend the algorithms to three dimensions; and because of the high accuracy obtainable on very coarse grids, reliable three-dimensional simulations should soon become practicable for routine engineering calculations.

ACKNOWLEDGMENTS

Portions of this work were supported by the National Science Foundation under contract ECS-8904595.

REFERENCES

1. Smith, R.M.; and Hutton, A.G.: The Numerical Treatment of Advection: A Performance Comparison of Current Methods. *Numer. Heat Trans.*, vol. **5**, 1982, pp. 439-461.

2. Spalding, D.B.: A Novel Finite Difference Formulation for Differential Expressions Involving Both First and Second Derivatives. *Int. J. Numer. Methods Eng.*, vol. **4**, 1972, pp. 551-559.

3. Patankar, S.V.: *Numerical Heat Transfer and Fluid Flow.* Hemisphere Publishing Corp., 1980.

4. Lewis, R.W.; and Morgan, K., eds.: *Numerical Methods in Thermal Problems*, **VI**, Pineridge Press, 1989.

5. Raithby, G.D.: A Critical Evaluation of Upstream Differencing Applied to Problems Involving Fluid Flow. *Comput. Methods Appl. Mech. Eng.*, vol. **9**, 1976, pp. 75-103.

6. Leonard, B.P.: A Consistency Check for Estimating Truncation Error Due to Upstream Differencing. *Appl. Math. Model.*, vol. **2**, 1978, pp. 239-244.

7. Leschziner, M.A.: Practical Evaluation of Three Finite Difference Schemes for the Computation of Steady-State Recirculating Flows. *Comput. Methods Appl. Mech. Eng.*, vol. **23**, 1980, pp. 293-312.

8. Huang, P.G.; Launder, B.E.; and Leschziner, M.A.: Discretization of Nonlinear Convection Processes: A Broad-Range Comparison of Four Schemes, *Comput. Methods Appl. Mech. Eng.*, vol. **48**, 1985, pp. 1-24.

9. Gaskell, P.H.; and Lau, A.K.C.: Curvature-Compensated Convective Transport: SMART, a New Boundedness Preserving Transport Algorithm, *Int. J. Numer. Methods Fluids*, vol. **8**, 1988, pp. 617-641.

10. Leonard, B.P.: Simple High Accuracy Resolution Program for Convective Modelling of Discontinuities. *Int. J. Numer. Methods Fluids*, vol. **8**, 1988, pp. 1291-1318.

11. Raithby, G.D.; and Schneider, G.E.: Elliptic Systems: Finite-Difference Method II. *Handbook of Numerical Heat Transfer*, W.J. Minkowycz, *et al.*, eds., Wiley, 1988, pp. 241-294.

12. Allen, D.N.deG.; and Southwell, R.V.: Relaxation Methods Applied to Determine the Motion, in Two Dimensions, of a Viscous Fluid Past a Fixed Cylinder. *Q. J. Mech. Appl. Math.*, vol. **8**, 1955, pp. 129-145.

13. Leonard, B.P.; and Mokhtari, S.: Beyond First-Order Upwinding: The ULTRA-SHARP Alternative for Non-Oscillatory Steady-State Simulation of Convection. *Int. J. Numer. Methods Eng.*, vol. **30**, 1990, pp. 729-766.

14. Leonard, B.P.: Elliptic Systems: Finite Difference Method IV. *Handbook of Numerical Heat Transfer*, W.J. Minkowycz, *et al.*, eds., Wiley, 1988, pp. 347-378.

15. Roe, P.L.; and Baines, M.J.: Algorithms for Advection and Shock Problems. *Proceedings of the 4th GAMM Conference on Numerical Methods in Fluid Mechanics*, H. Viviand, ed., Vieweg, West Germany, 1982, pp. 281-290.

16. Sweby, P.K.: High Resolution Schemes Using Flux Limiters for Hyperbolic Conservation Laws. *SIAM J. Numer. Anal.*, vol. **21**, 1984, pp. 995-1011.

17. Tzanos, C.P.: Central Difference-Like Approximation for the Solution of the Convection-Diffusion Equation. *Numer. Heat Trans.*, Part B, vol. **17**, 1990, pp. 97-112.

18. Mokhtari, S.: Development and Analysis of Steady High-Resolution Non-Oscillatory Convection Schemes Using Higher-Order Upwinding. Ph.D. Dissertation, The University of Akron, 1991.

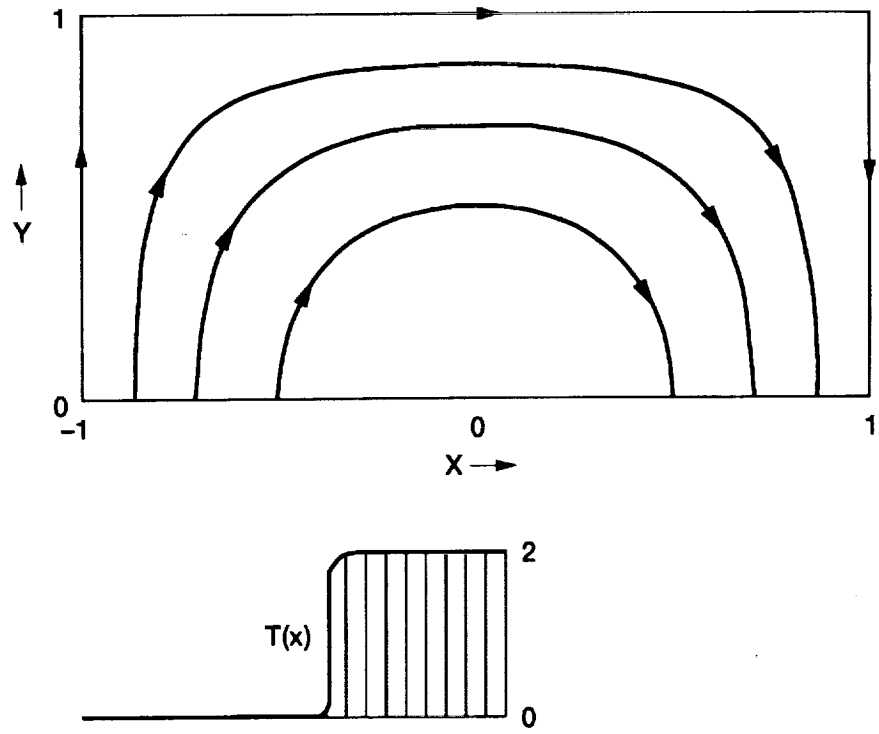

Figure 1.—Streamline pattern and inlet temperature profile.

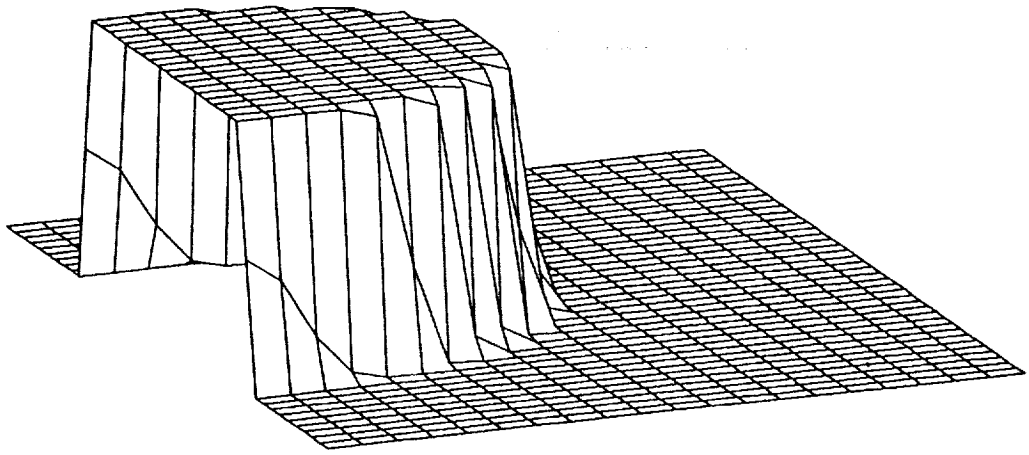

(a) $\alpha = 100.$

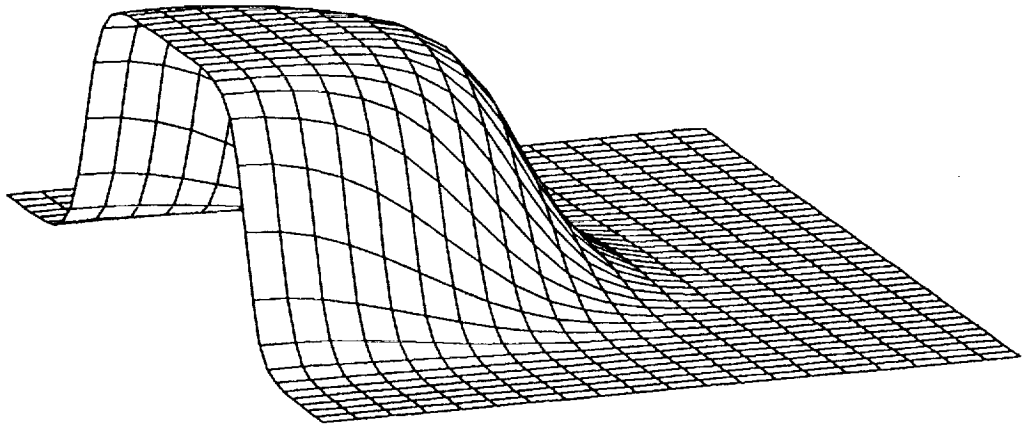

(b) $\alpha = 5.$

Figure 2.—Three-dimensional portrayal of $T(x,y)$ for the infinite-Pe solution.

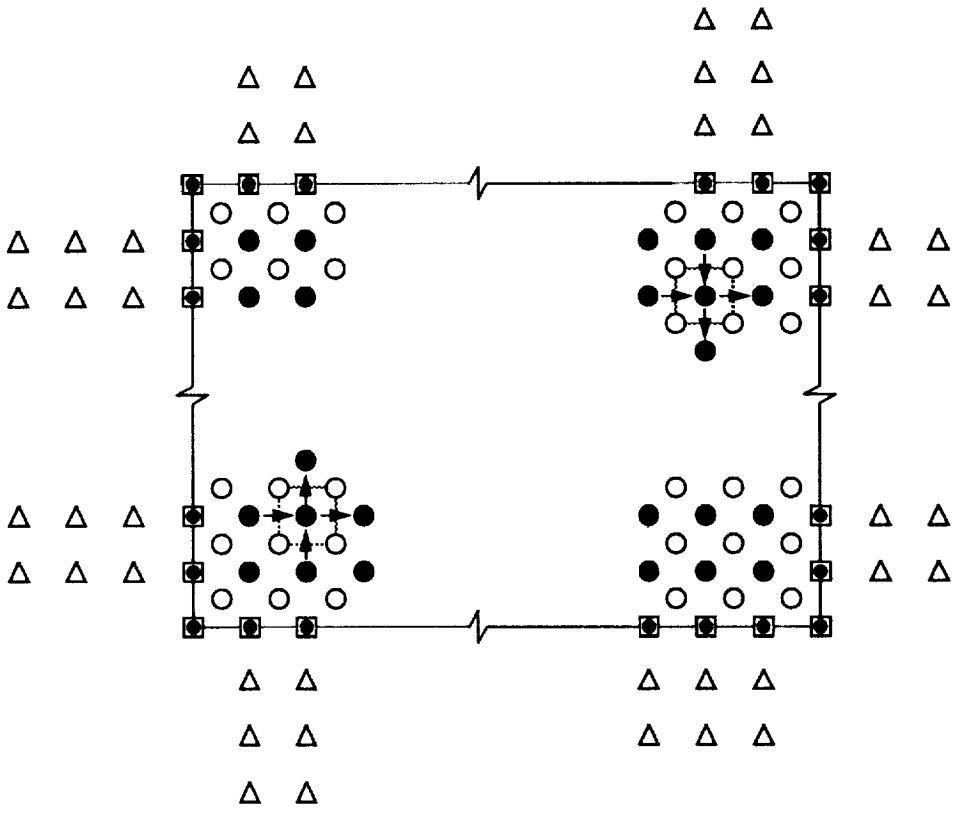

Figure 3.—Schematic of staggered mesh. Hollow circles are stream-function nodes. Solid dots are temperature nodes. Triangles represent external pseudo-nodes for temperature.

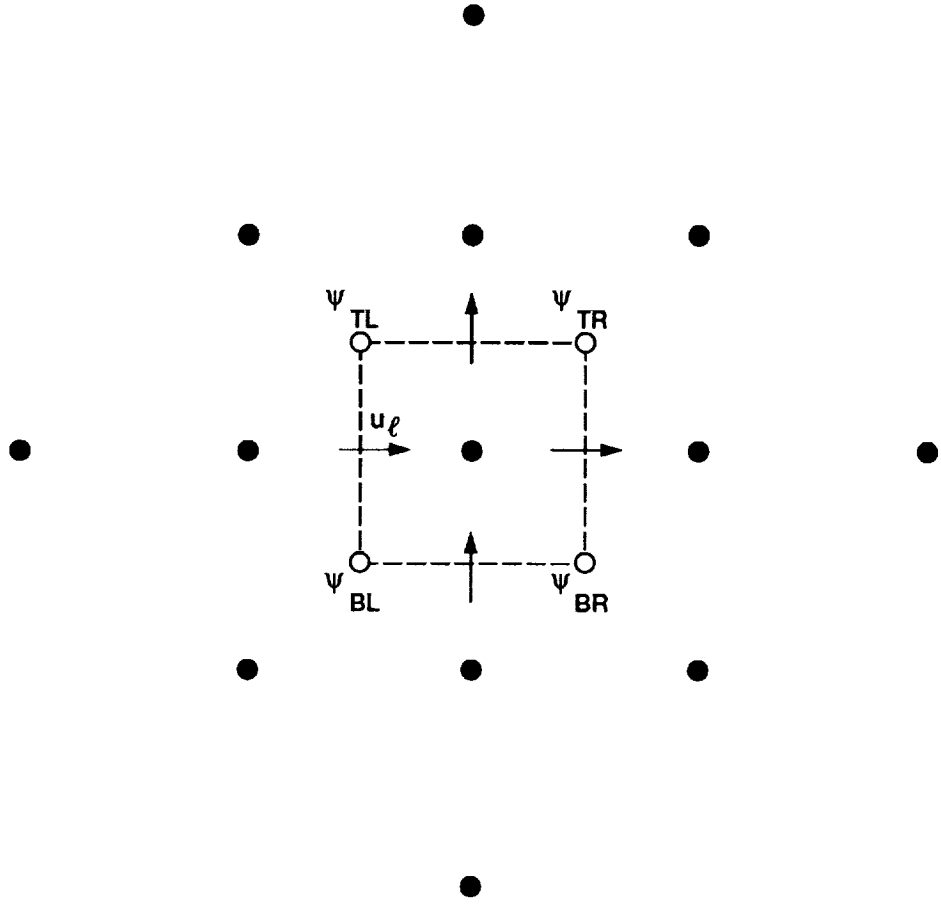

Figure 4.—Detail of typical internal control-volume cell for the temperature transport equation.

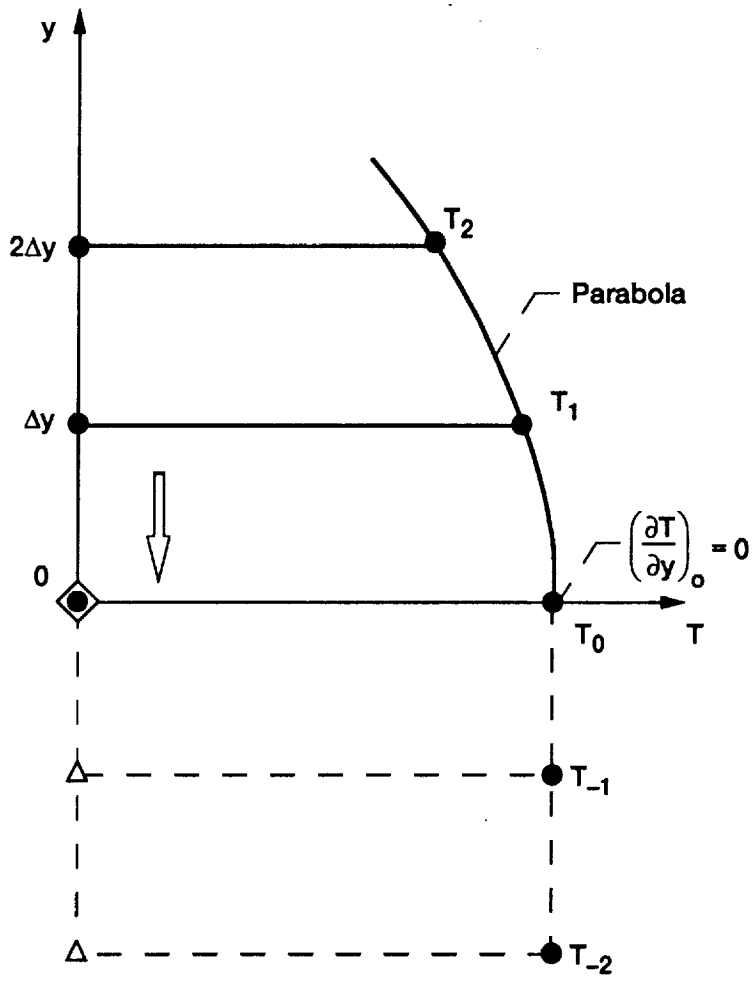

Figure 5.—Outflow numerical boundary-condition treatment. T_0 is determined by interpolating a parabola through T_2 and T_1 so that $(\partial T/\partial y)_0 = 0$.

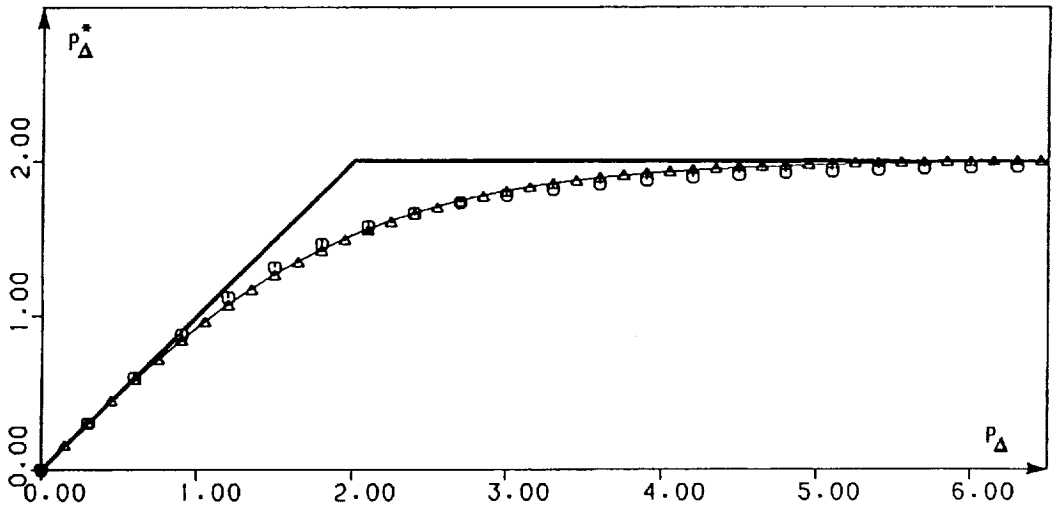

Figure 6.—Comparison of Spalding's (piece-wise linear) Hybrid method, Patankar's power-law scheme (triangles), and Raithby-and-Schneider's algebraic approximation (circles) with the exponential-differencing scheme (light continuous curve).

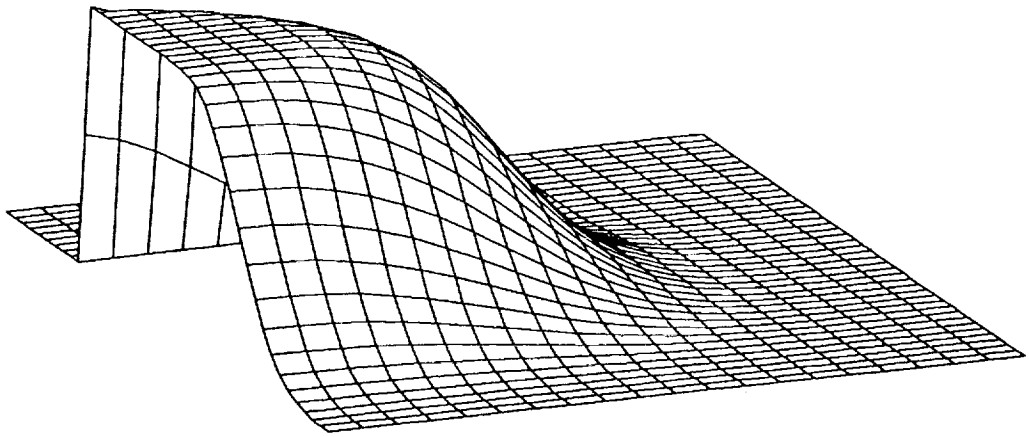

(a) $\alpha = 100$, $\mathscr{C} = 0.135$.

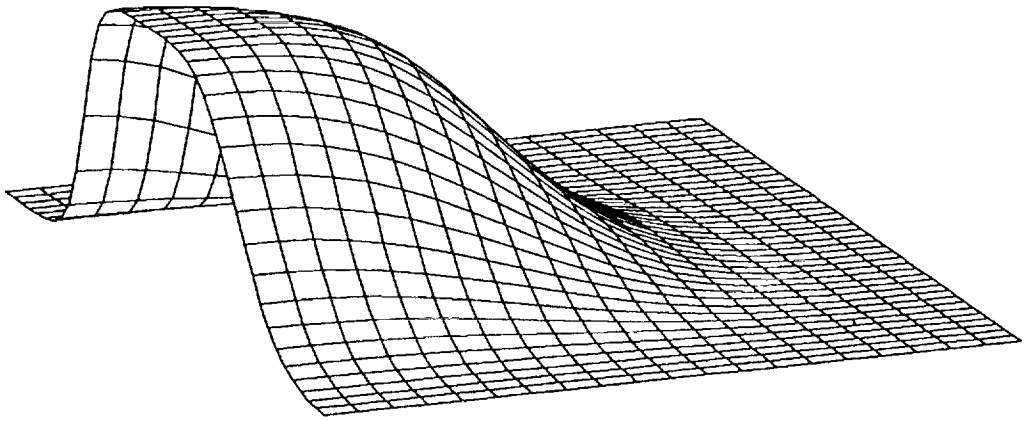

(b) $\alpha = 5$, $\mathscr{C} = 0.073$.

Figure 7.—Infinite-Pe results for exponential-based schemes (equivalent to first-order upwinding) on a 40x20 mesh.

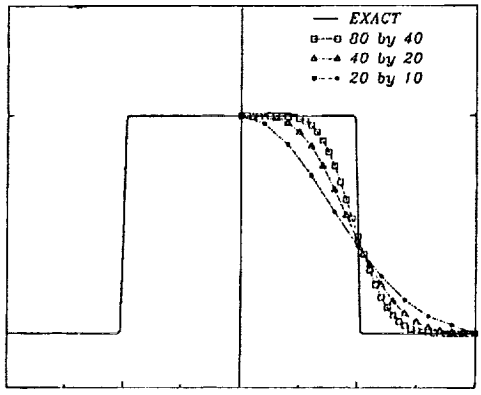

(a) Pe = ∞.

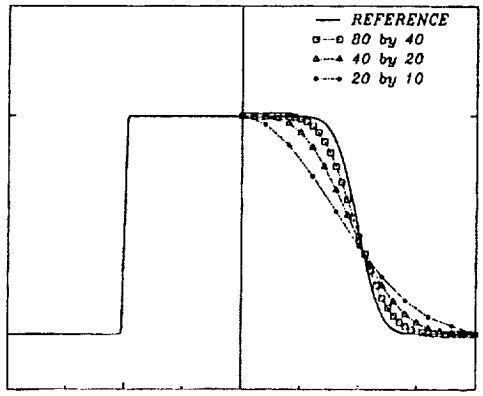

(b) Pe = 500.

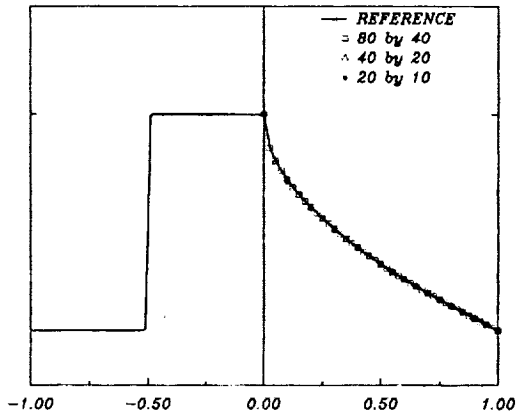

(c) Pe = 10.

Figure 8.—Inlet and outlet temperature profiles for α = 100 using PLDS.

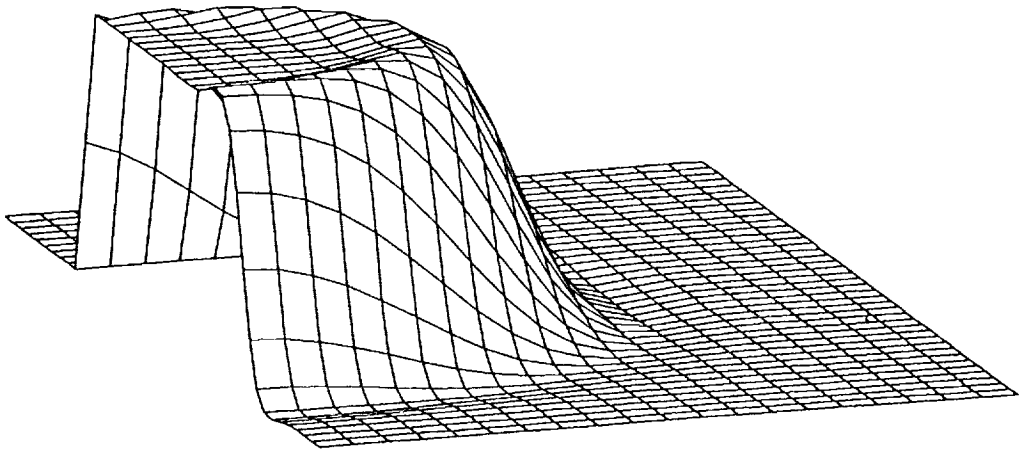

(a) $\alpha = 100$, $\mathscr{E} = 0.062$.

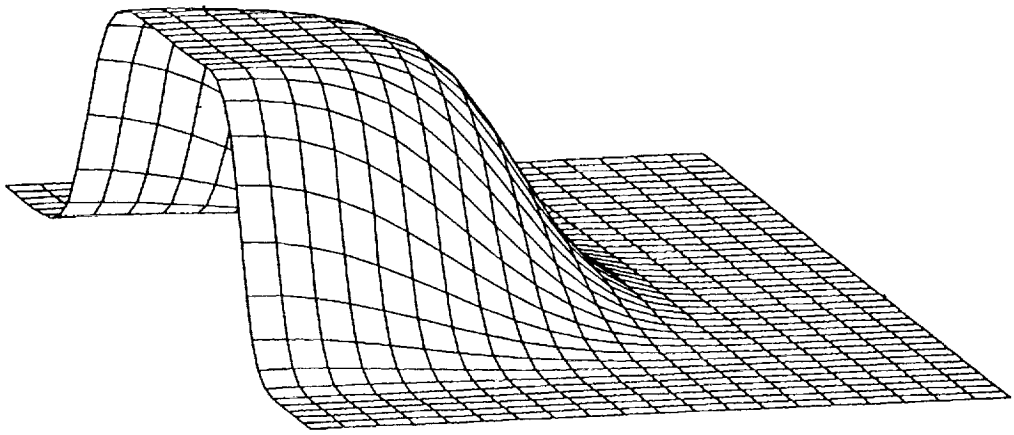

(b) $\alpha = 5$, $\mathscr{E} = 0.014$.

Figure 9.—Infinite-Pe results for second-order upwinding on a 40x20 mesh.

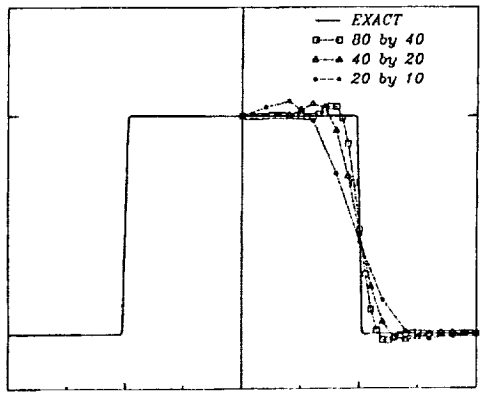

(a) Pe = ∞.

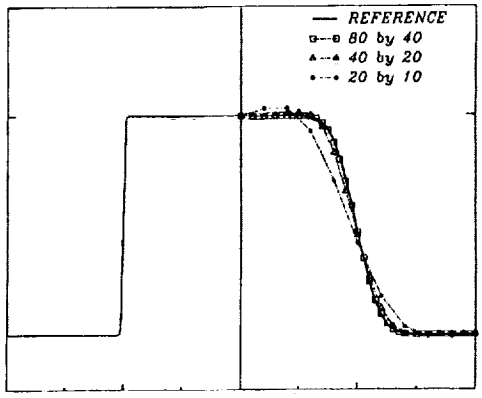

(b) Pe = 500.

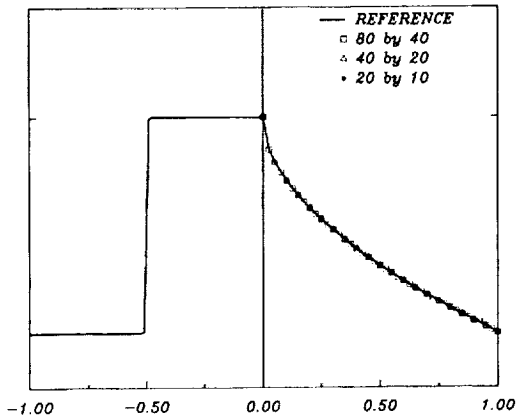

(c) Pe = 10.

Figure 10.—Inlet and outlet profiles for $\alpha = 100$ using second-order upwinding.

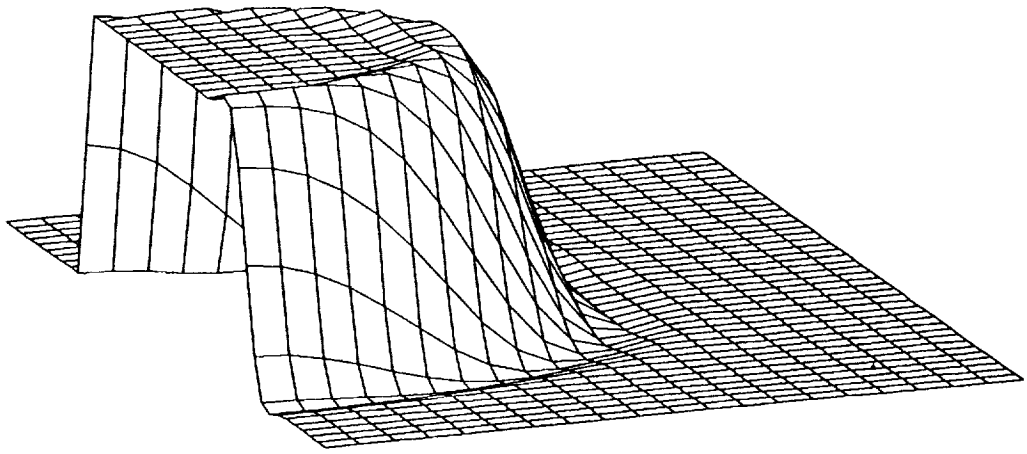

(a) $\alpha = 100, \mathscr{E} = 0.045$.

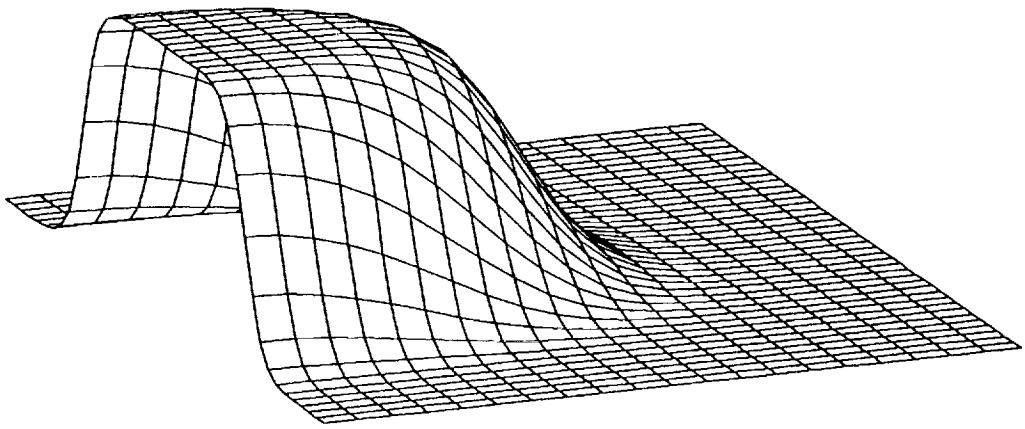

(b) $\alpha = 5, \mathscr{E} = 0.005$.

Figure 11.—Infinite-Pe results using the QUICK scheme on a 40x20 mesh.

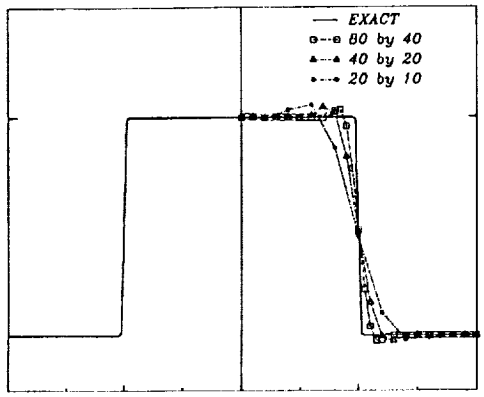

(a) Pe = ∞.

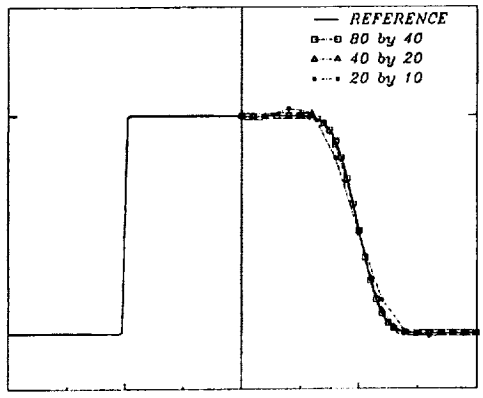

(b) Pe = 500.

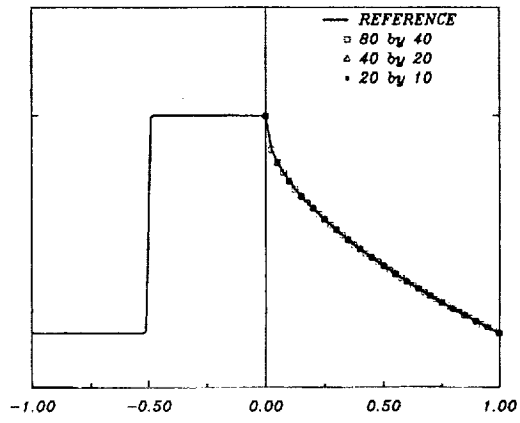

(c) Pe = 10.

Figure 12.—Inlet and outlet profiles for α = 100 using the QUICK scheme.

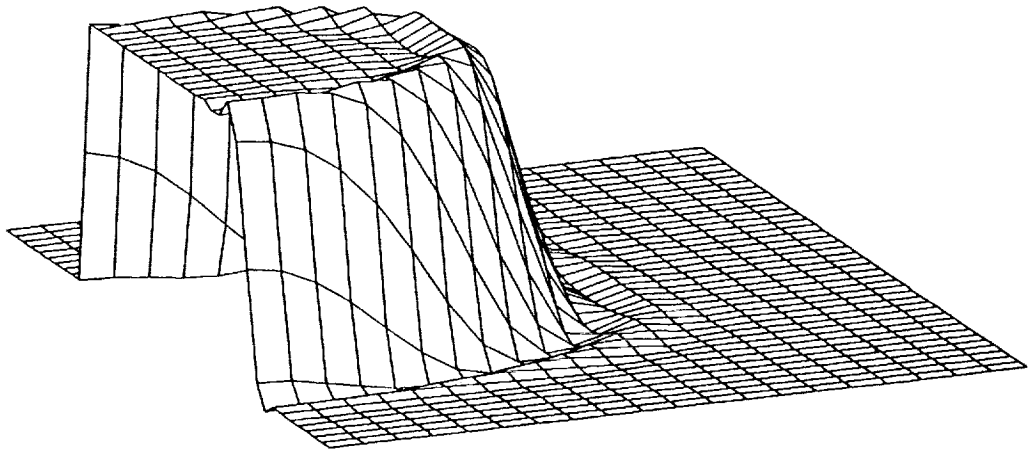

(a) $\alpha = 100$, $\mathscr{C} = 0.036$.

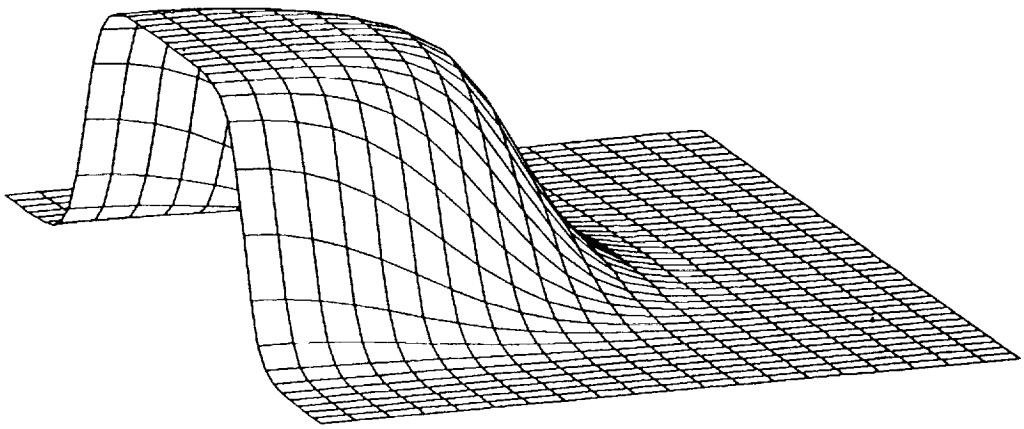

(b) $\alpha = 5$, $\mathscr{C} = 0.003$.

Figure 13.—Infinite-Pe results using fifth-order upwinding on a 40x20 mesh.

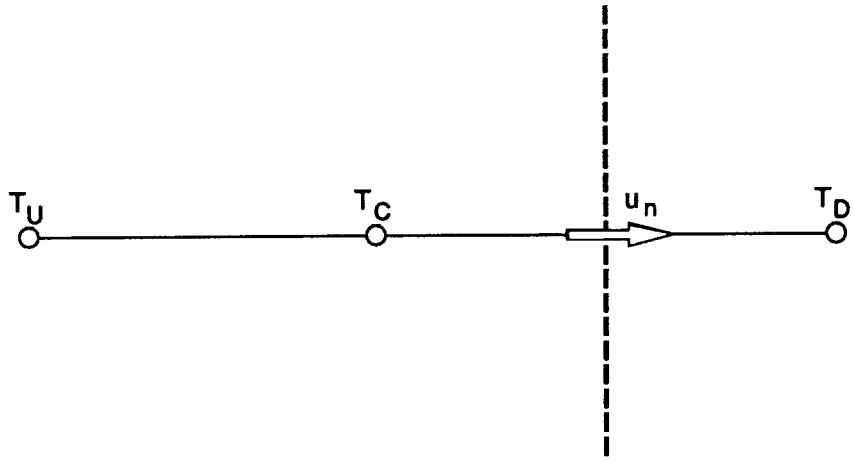

Figure 14.—Definition of downwind (D), upwind (U) and central (C) nodes according to the direction of u_n at a control-volume face.

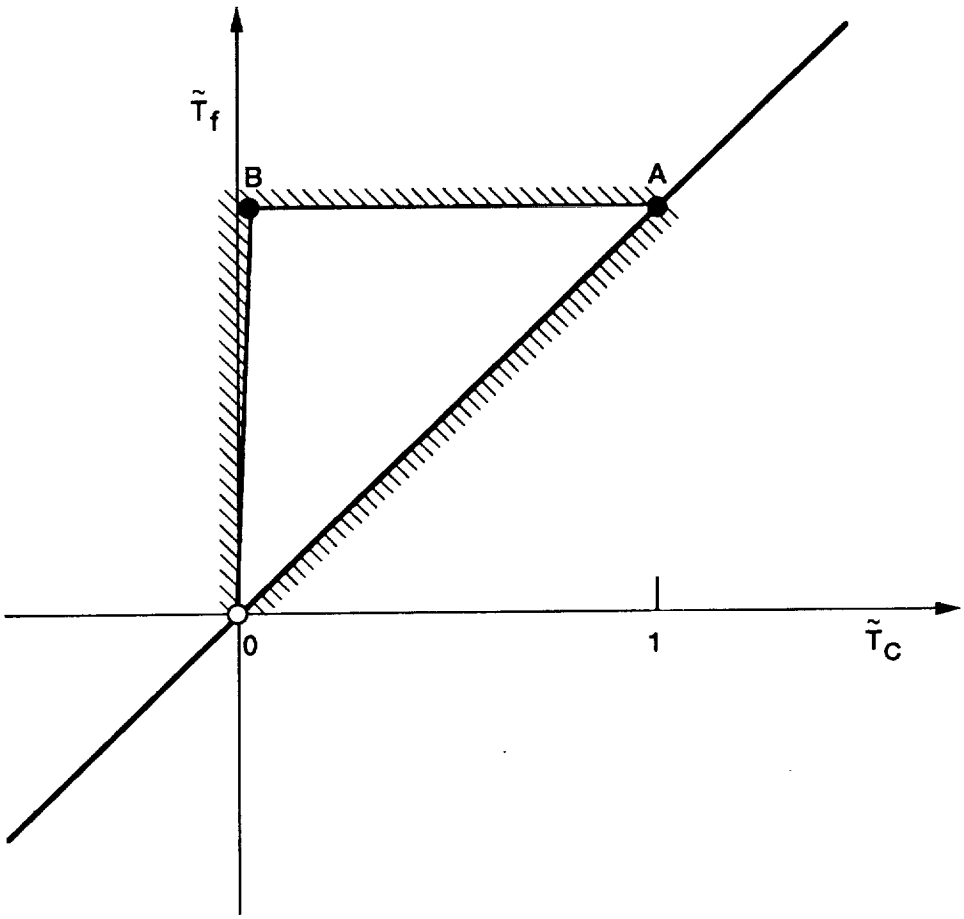

Figure 15.—Portrayal of the universal-limiter constraints in the normalized-variable diagram.

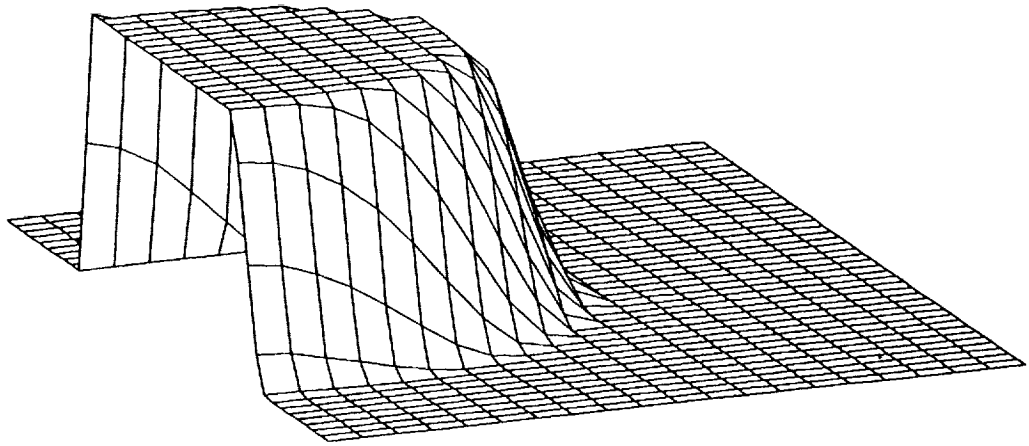

(a) $\alpha = 100, \mathscr{E} = 0.034$.

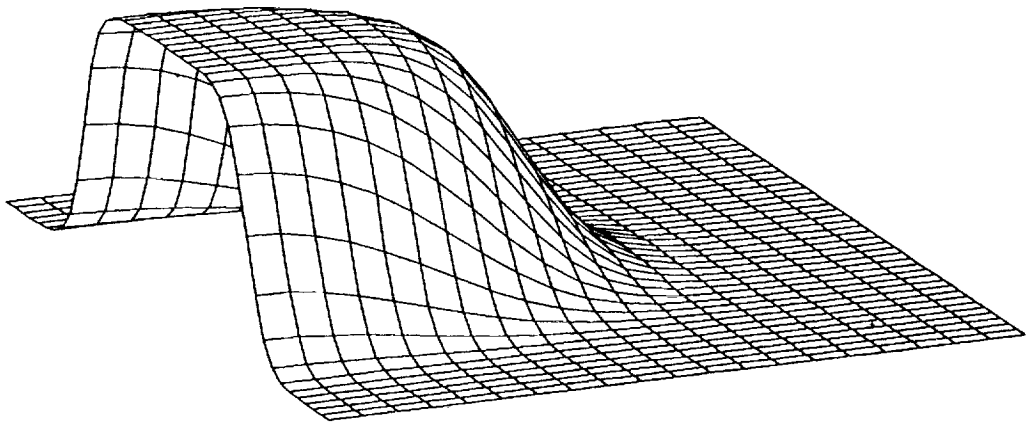

(b) $\alpha = 5, \mathscr{E} = 0.005$.

Figure 16.—Infinite-Pe results using ULTRA-QUICK on a 40x20 mesh.

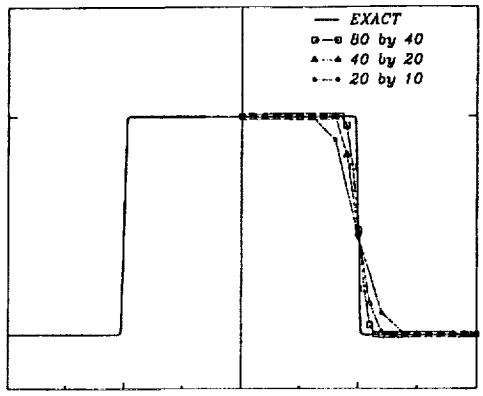

(a) Pe = ∞.

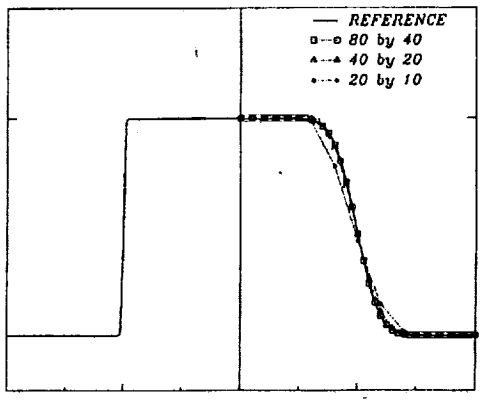

(b) Pe = 500.

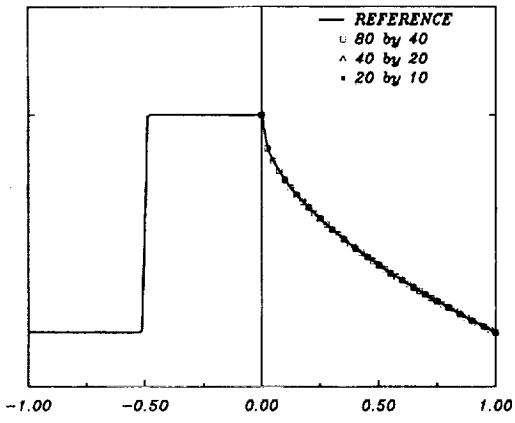

(c) Pe = 10.

Figure 17.—Inlet and outlet profiles for $\alpha = 100$ using the ULTRA-QUICK scheme.

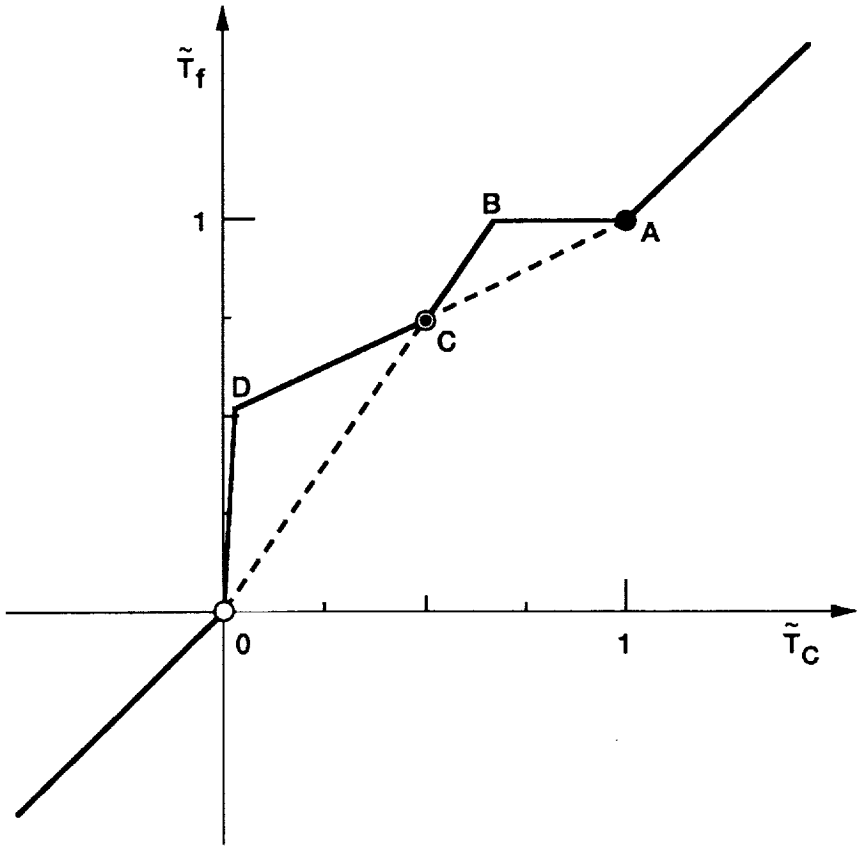

Figure 18.—The Ultra-B scheme portrayed in the normalized-variable diagram.

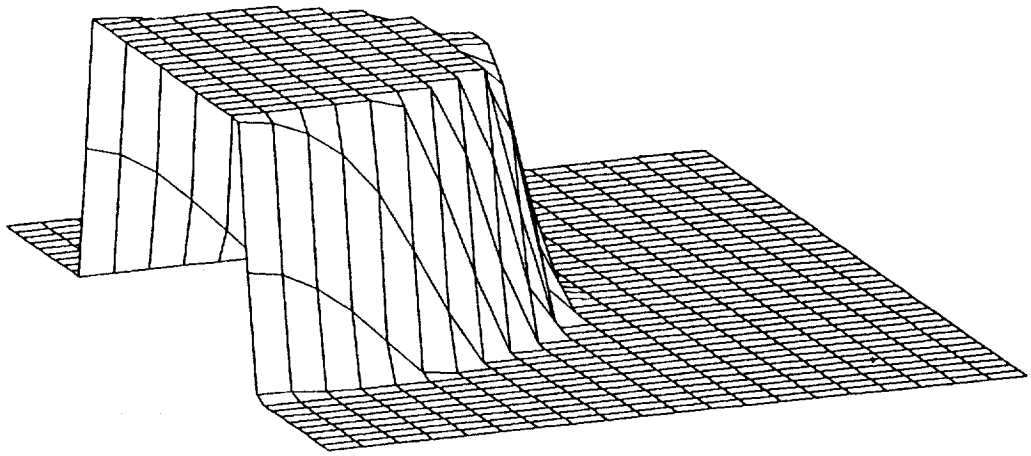

(a) $\alpha = 100, \mathscr{C} = 0.024$.

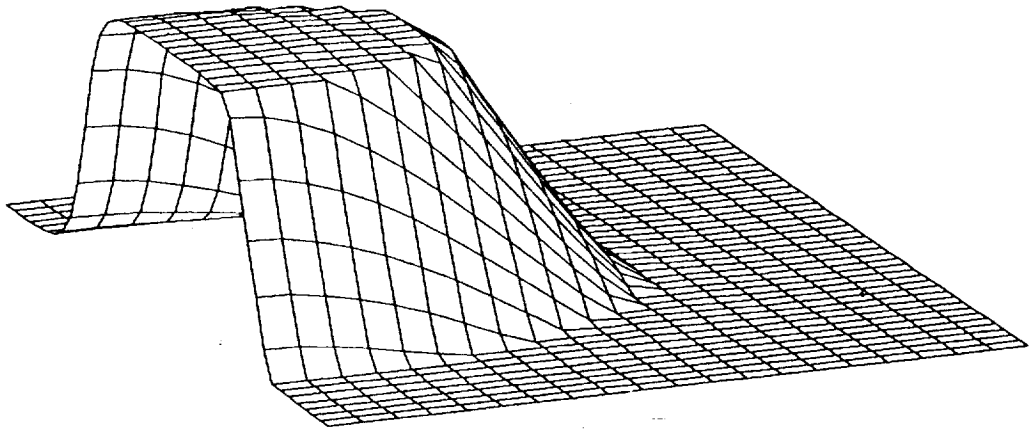

(b) $\alpha = 5, \mathscr{C} = 0.013$.

Figure 19.—Infinite-Pe results using the Ultra-B scheme on a 40x20 mesh. Note the artificial steepening and clipping in case (b).

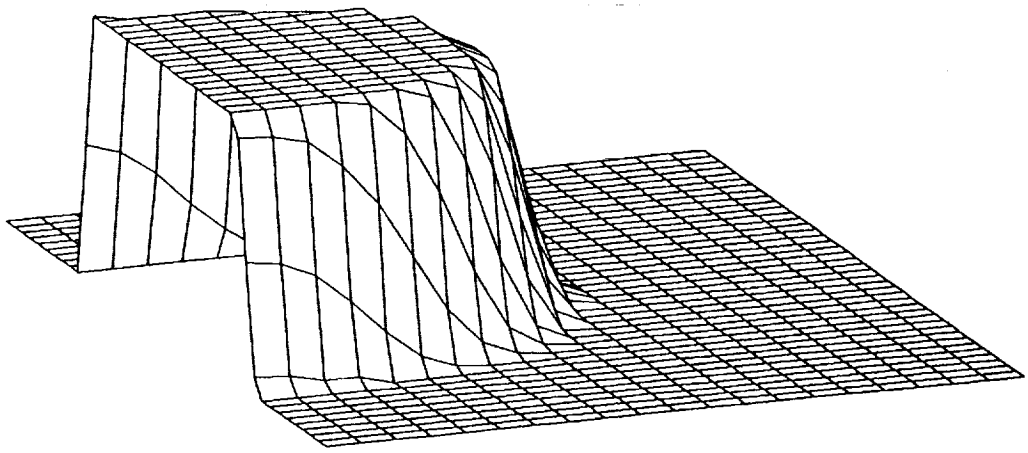

(a) $\alpha = 100$, $\mathscr{E} = 0.024$.

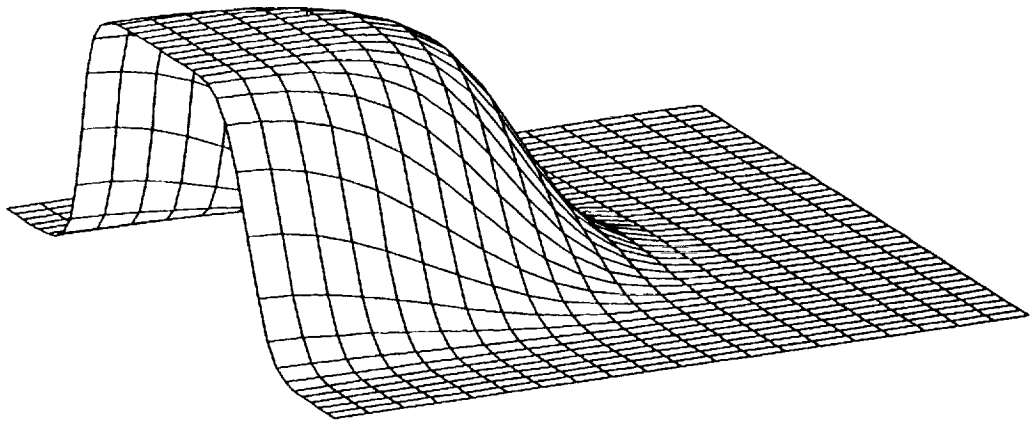

(b) $\alpha = 5$, $\mathscr{E} = 0.004$.

Figure 20.—Infinite-Pe results using the ULTRA-3/5/7 adaptive-stencil-expansion method on a 40x20 mesh.

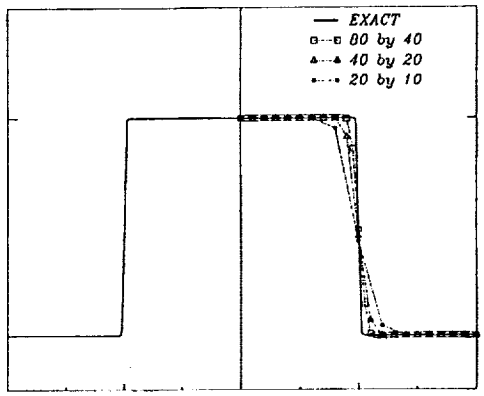

(a) Pe = ∞.

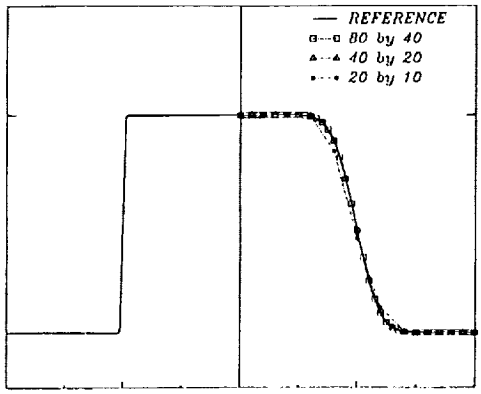

(b) Pe = 500.

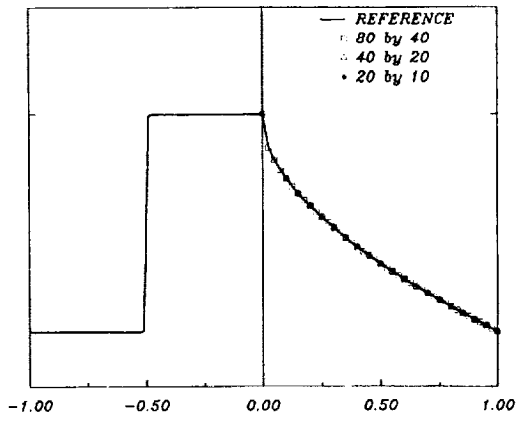

(c) Pe = 10.

Figure 21.—Inlet and outlet profiles for α = 100 using ULTRA-3/5/7.

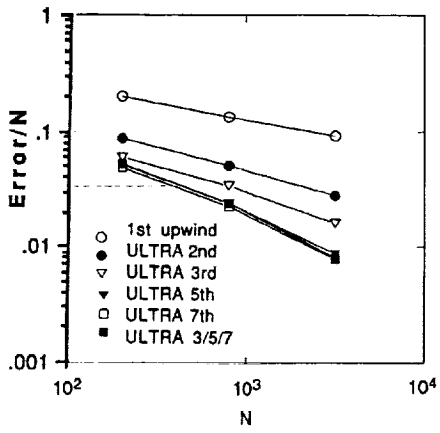

(a) Error *versus* grid refinement.

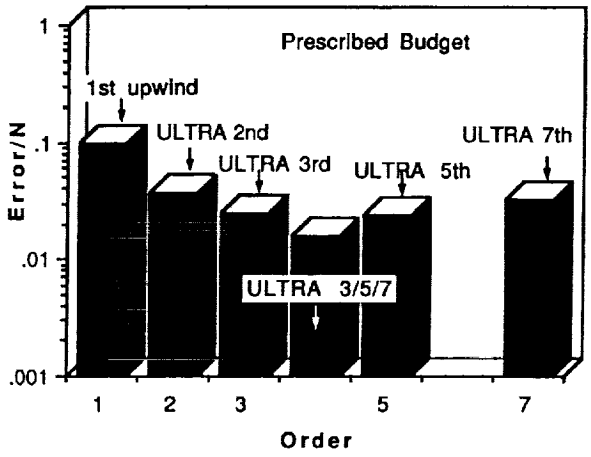

(c) Error for a prescribed budget.

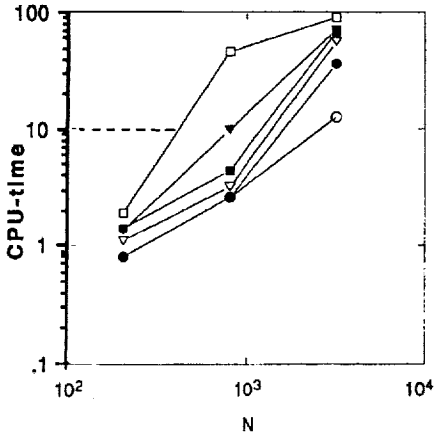

(b) Cost *versus* grid refinement.

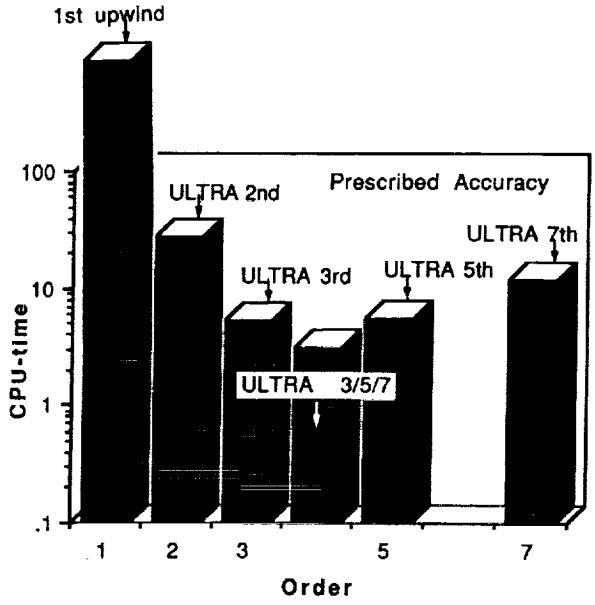

(d) Cost for a prescribed accuracy.

Figure 22.—Computational efficiency of various nonoscillatory schemes for $\alpha = 100$ and $Pe = \infty$.

REPORT DOCUMENTATION PAGE

Form Approved
OMB No. 0704-0188

1. AGENCY USE ONLY (*Leave blank*)	2. REPORT DATE	3. REPORT TYPE AND DATES COVERED
	February 1992	Technical Memorandum

4. TITLE AND SUBTITLE

ULTRA-SHARP Solution of the Smith-Hutton Problem

5. FUNDING NUMBERS

WU-505-62-21

6. AUTHOR(S)

B.P. Leonard and Simin Mokhtari

7. PERFORMING ORGANIZATION NAME(S) AND ADDRESS(ES)

National Aeronautics and Space Administration
Lewis Research Center
Cleveland, Ohio 44135-3191

8. PERFORMING ORGANIZATION REPORT NUMBER

E-6393

9. SPONSORING/MONITORING AGENCY NAMES(S) AND ADDRESS(ES)

National Aeronautics and Space Administration
Washington, D.C. 20546-0001

10. SPONSORING/MONITORING AGENCY REPORT NUMBER

NASA TM-105435
ICOMP-92-03

11. SUPPLEMENTARY NOTES

B.P. Leonard, Institute for Computational Mechanics in Propulsion, Lewis Research Center (Work Funded by Space Act Agreement C-99066-G). Space Act Monitor: Louis A. Povinelli, Simin Mokhtari, Dept. of Mechanical Engineering, The University of Akron, Akron, Ohio 44325.

12a. DISTRIBUTION/AVAILABILITY STATEMENT

Unclassified - Unlimited
Subject Category 34

12b. DISTRIBUTION CODE

13. ABSTRACT ***(Maximum 200 words)***

Highly convective scalar transport involving near-discontinuities and strong streamline curvature was addressed in a paper by Smith and Hutton in 1982, comparing several different convection schemes applied to a specially devised test problem. First-order methods showed significant artificial diffusion, whereas higher-order methods gave less smearing but had a tendency to overshoot and oscillate. Perhaps because unphysical oscillations are more obvious than unphysical smearing, the intervening period has seen a rise in popularity of low-order artificially diffusive schemes, especially in the numerical heat-transfer industry. The present paper describes an alternative strategy of using non-artificially diffusive higher-order methods, while maintaining strictly monotonic transitions through the use of simple flux-limited constraints. Limited third-order upwinding is usually found to be the most cost-effective basic convection scheme. Tighter resolution of discontinuities can be obtained at little additional cost by using automatic adaptive stencil expansion to higher order in local regions, as needed.

14. SUBJECT TERMS

Convective heat-transfer; ULTRA-SHARP

15. NUMBER OF PAGES

40

16. PRICE CODE

A03

17. SECURITY CLASSIFICATION OF REPORT	18. SECURITY CLASSIFICATION OF THIS PAGE	19. SECURITY CLASSIFICATION OF ABSTRACT	20. LIMITATION OF ABSTRACT
Unclassified	Unclassified	Unclassified	